Li$_2$HgMS$_4$ (M = Si, Ge, Sn): New Quaternary Diamond-Like Semiconductors for Infrared Laser Frequency Conversion

Kui Wu and Shilie Pan *

Key Laboratory of Functional Materials and Devices for Special Environments of CAS,
Xinjiang Key Laboratory of Electronic Information Materials and Devices,
Xinjiang Technical Institute of Physics & Chemistry of CAS, 40-1 South Beijing Road,
Urumqi 830011, China; wukui@ms.xjb.ac.cn
* Correspondence: slpan@ms.xjb.ac.cn; Tel.: +86-991-3674558

Abstract: A new family of quaternary diamond-like semiconductors (DLSs), Li$_2$HgMS$_4$ (M = Si, Ge, Sn), were successfully discovered for the first time. All of them are isostructural and crystallize in the polar space group (*Pmn*2$_1$). Seen from their structures, they exhibit a three-dimensional (3D) framework structure that is composed of countless 2D honeycomb layers stacked along the *c* axis. An interesting feature, specifically, that the LiS$_4$ tetrahedra connect with each other to build a 2D layer in the *ac* plane, is also observed. Experimental investigations show that their nonlinear optical responses are about 0.8 for Li$_2$HgSiS$_4$, 3.0 for Li$_2$HgGeS$_4$, and 4.0 for Li$_2$HgSnS$_4$ times that of benchmark AgGaS$_2$ at the 55–88 μm particle size, respectively. In addition, Li$_2$HgSiS$_4$ and Li$_2$HgGeS$_4$ also have great laser-damage thresholds that are about 3.0 and 2.3 times that of powdered AgGaS$_2$, respectively. The above results indicate that title compounds can be expected as promising IR NLO candidates.

Keywords: nonlinear optical materials; crystal structure; good NLO responses

1. Introduction

Solid-state lasers have shown a wide range of applications in the fields of military, industry, medical treatment and information communications [1,2]. However, traditional laser sources, such as Ti:Al$_2$O$_3$ and Nd:YAG lasers, mainly cover the wavelengths range from visible to near infrared, not including the important ultraviolet (UV < 400 nm) and middle-far infrared (MFIR, 3–20 μm) region [3,4]. To extend the laser wavelength ranges, frequency-conversion technology on nonlinear optical (NLO) materials was invented and has been further developed for decades [5]. Recently, many promising NLO materials have been discovered and have basically solved the demand of UV region [6–34]. However, for the IR region, outstanding IR NLO materials were rarely discovered and only several ternary diamond-like semiconductors (DLSs), such as AgGaS$_2$, AgGaSe$_2$ and ZnGeP$_2$, have been commercially used [35–37]. Although they have high second harmonic generation (SHG) coefficients and wide IR transmission regions, some of the self-defects including the low laser-damage thresholds (LDTs) or strong two-photon absorption (TPA) still seriously hinder their practical application. Researchers have done a lot of work to explore new NLO materials for the IR application, and the combination of two or more different building units into crystal structures can be viewed as a feasible way to obtain new NLO compounds. Up to now, many reports indicate that cations with second order Jahn–Teller distortions, lone electron pairs or d^{10} configuration can contribute to good SHG response with the cooperative effects of typical tetrahedral

units MQ$_4$ (M = Ga, In, Si, Ge, Sn; Q = S, Se) [38–73]. Note that diamond-like semiconductors (DLSs) with inherently noncentrosymmetrical (NCS) structures, with all the tetrahedral units in crystal structures oriented in the same direction, have been further investigated on the ternary and quaternary systems [74–80]. Among them, the d^{10} cations (Zn^{2+}, Cd^{2+}) containing quaternary DLSs with outstanding performances, such as Li$_2$CdGeS$_4$, Li$_2$ZnGeSe$_4$, and Li$_2$ZnSnSe$_4$ [74,78], were proven as promising IR NLO candidates and belong to the general formula I$_2$–II–IV–VI$_4$, where I are the monovalent elements, II are the divalent elements, IV are the group 14 elements, and VI are the chalcogen elements. Previous reports indicate that other types of Hg-containing metal chalcogenides have shown good NLO performances in the IR field, such as HgGaS$_4$ [81]. BaHgQ$_2$ (Q = S, Se), [82,83] A$_2$Hg$_3$M$_2$S$_8$ (A = Na, K; M = Si, Ge, Sn) [61,68], and Li$_4$HgGe$_2$S$_7$ [84]. However, up to now, the Hg-containing DLSs have been rarely investigated in the IR frequency conversion region. Thus, it is meaningful to explore new Hg-containing DLSs and study their important NLO properties. From this background, we have chosen the Li–Hg–M–S (M = Si, Ge, Sn) as the research system and successfully prepared three new IR NLO materials, Li$_2$HgMS$_4$ (M = Si, Ge, Sn). They are isostructural and crystallize in the *Pmn*2$_1$ polar space group. Overall properties investigation shows that they can be expected to be promising IR NLO candidates owing to their large NLO coefficients, high LDTs, wide IR transparent regions, and good chemical stability.

2. Results and Discussion

2.1. Crystal Structure

The title compounds are isostructural and crystallize in the NCS polar space group *Pmn*2$_1$. In order to ensure the reasonability of crystal structures of title compounds, the bond valence [85,86] and the global instability index (GII) [87–89] were also systemically studied (Table 1). Calculated results (Li, 1.085–1.125; Hg, 2.090–2.133; Si/Ge/Sn, 4.030–4.152; S, 2.055–2.229) indicate that all atoms are in reasonable oxidation states. In addition, GII can be derived from the bond valence concepts, which represent the tension of lattice parameters and are always used to evaluate the rationality of structure. When the value of GII is less than 0.05 vu (valence unit), the tension of structure is not proper, whereas when the value of GII is larger than 0.2 vu, its structure is not stable. Thus, the value of GII in a reliable structure should be limited at 0.05–0.2 in general. As for the title compounds, calculated GII values are in the range of 0.10–0.14 vu, which illustrates that the crystal structures of all compounds are reasonable.

Table 1. Bond Valence Sum (vu) and Global Instability Index (GII) of title compounds.

| Compounds	Li$^+$	Hg^{2+}	Si/Ge/Sn^{4+}	S^{2-}	GII
Li$_2$HgSiS$_4$	1.125	2.092	4.030	2.069–2.149	0.10
Li$_2$HgGeS$_4$	1.118	2.090	4.152	2.055–2.229	0.14
Li$_2$HgSnS$_4$	1.085	2.133	4.138	2.061–2.163	0.13

Herein, Li$_2$HgGeS$_4$ is chosen as the representative for the structural discussion. In its structure, each cation is linked to four S atoms, forming the typical LiS$_4$, HgS$_4$, and GeS$_4$ tetrahedra. These units connect with each other to make up a two-dimensional (2D) honeycomb layer structure, which is located at the *ab* plane (Figure 1b). Then, the layers are further stacked along the *c* axis to form a three-dimensional (3D) framework structure (Figure 1a). In addition, an interesting feature is that the LiS$_4$ tetrahedra connect with each other to build a 2D layer in the *ac* plane (Figure 1c). The whole structure is composed of tetrahedral ligands that align along the *c* axis. Note that the discovered quaternary DLSs in the I$_2$–II–IV–VI$_4$ systems normally crystallize in the one of following space groups: *I*-42*m* (Cu$_2$CdSnS$_4$) [76], *I*-4 (Cu$_2$ZnSnS$_4$) [90], *Pmn*2$_1$ (Li$_2$CdGeS$_4$) [74], *Pna*2$_1$ (Li$_2$MnGeS$_4$) [75], and *Pn* (Li$_2$CoSnS$_4$) [75], to our best knowledge, which represent the stannite, kesterite, wurtz-stannite, and wurtz-kesterite structural features.
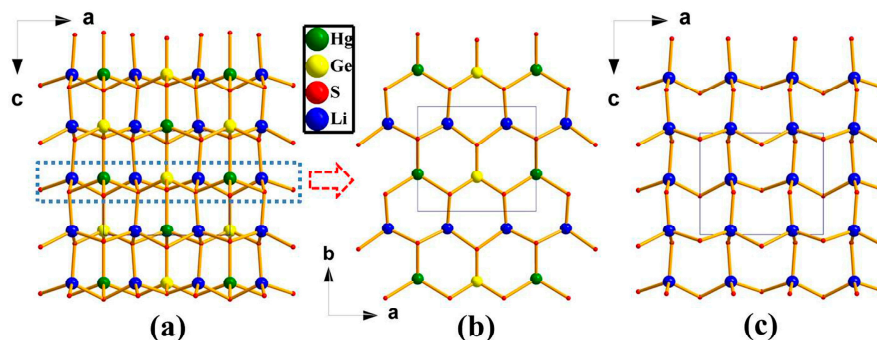
Figure 1. (**a**) View of the crystal structure of Li_2HgGeS_4 along the *b* axis; (**b**) A honeycomb-like layer composed of the LiS_4, HgS_4, and GeS_4 units located at the *ab* plane; (**c**) A layer composed of the LiS_4 units located at the *ac* plane.

2.2. Optical Properties

As for an IR NLO crystal, its optical parameters, such as optical bandgap, IR absorption edge, NLO response, and LDT, are necessary to be determined for the assessment of application prospect. The detailed mechanism for laser damage in a given material is not fully clear yet, however it has been normally accepted that strong optical absorption of the materials will cause thermal and electronic effects and finally lead to laser damage. Note that the optical breakdown can be attributed to the effect of electron avalanche that has a close relationship with optical bandgap in a given material [75]. Figure 2 shows that the optical bandgaps are 2.68 for Li_2HgSiS_4, 2.46 for Li_2HgGeS_4, and 2.32 eV for Li_2HgSnS_4, respectively. All of them are much larger than those of commercial $AgGaSe_2$ (1.80 eV) [86] and $ZnGeP_2$ (1.75 eV) [37], which may be conducive to improve the laser damage resistance of the title compounds compared with the commercially available IR NLO materials. Recently, the assessment of the LDTs on powder samples has been developed as a feasible and semi-quantitative method [52,55]. Thus, in this work, based on a pulse laser (1.06 μm, 10 Hz and 10 ns), the LDTs of the title compounds were measured with $AgGaS_2$ as the reference and corresponding results are shown in Table 2. From this table, it can be found that the title compounds have great LDTs, such as 91.6 for Li_2HgSiS_4, 70.6 for Li_2HgGeS_4, and 30.5 MW/cm^2 for Li_2HgSnS_4, and are about 3.0, 2.3, and ~1 times that of powdered $AgGaS_2$ (29.6 MW/cm^2), respectively. Moreover, Li_2HgSiS_4 and Li_2HgGeS_4 are comparable to those of $PbGa_2GeSe_6$ (3.7 × $AgGaS_2$) [51], $Na_2In_2GeS_6$ (4.0 × $AgGaS_2$) [56], $Na_2Hg_3Ge_2S_8$ (3 × $AgGaS_2$) [61], and $SnGa_4Se_7$ (4.6 × $AgGaS_2$) [52]. Therefore, Li_2HgSiS_4 and Li_2HgGeS_4 can be expected to have application with high-power lasers, compared with the commercial IR NLO materials.
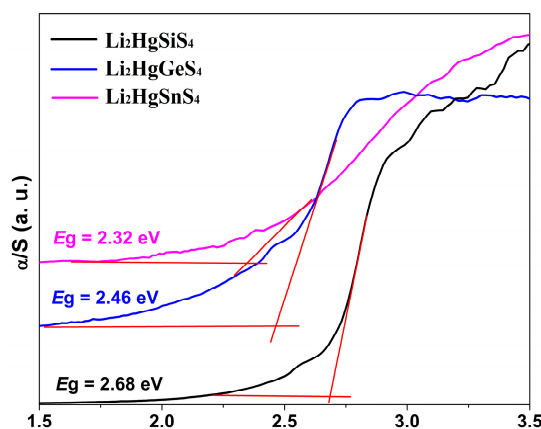

**Figure 2.** Experimental bandgaps of the title compounds.

Table 2. LDTs of the title compounds and AgGaS$_2$ (as the reference).

Compounds	Damage Energy (mJ)	Spot Diameter (mm)	LDT (MW/cm^2)
AgGaS$_2$	0.33	0.375	29.6
Li$_2$HgSiS$_4$	1.02	0.375	91.6
Li$_2$HgGeS$_4$	0.78	0.375	70.2
Li$_2$HgSnS$_4$	0.34	0.375	30.5

In addition, Raman spectra (Figure 3) are also measured to determine the IR absorption edges for the title compounds. The results show that all of them exhibit the wide IR transmission regions, such as 2.5–19 μm (530 cm^{-1}) for Li$_2$HgSiS$_4$, 2.5–22 μm (450 cm^{-1}) for Li$_2$HgGeS$_4$, and 2.5–23.5 μm (425 cm^{-1}) for Li$_2$HgSnS$_4$, which cover the two important atmospheric windows (3–5 and 8–12 μm) that can be used in telecommunications, laser guidance, and explosives detection. Note that the IR absorption edges gradually get longer from the Si to Sn compounds, which are consistent with the IR data for other related mental chalcogenides [61]. Although the measured IR absorption data on powder samples have some deviations with the results on single-crystals, they can give the preliminary assessment for the transmission region of IR materials. Overall view on Raman spectra shows similar patterns for the title compounds, and a shift to lower absorption energies from the Si to Sn compounds that are severely affected by the tetravalent (M^{IV}) metals. The absorption peaks above approximately 300 cm^{-1}, including Li$_2$HgSiS$_4$ (520, 396 cm^{-1}), Li$_2$HgGeS$_4$ (430, 387, 360, 327 cm^{-1}), and Li$_2$HgSnS$_4$ (402, 346 cm^{-1}), can be assigned to the characteristic absorptions of the Si–S, Ge–S, and Sn–S modes, respectively. Moreover, several peaks located between 200 and 300 cm^{-1}, such as Li$_2$HgSiS$_4$ (285, 258 cm^{-1}), Li$_2$HgGeS$_4$ (257 cm^{-1}), and Li$_2$HgSnS$_4$ (258 cm^{-1}), are attributed to the Hg–S bonding interactions. In addition, the absorptions below 200 cm^{-1} are primarily corresponding to the Li–S vibrations for the title compounds.
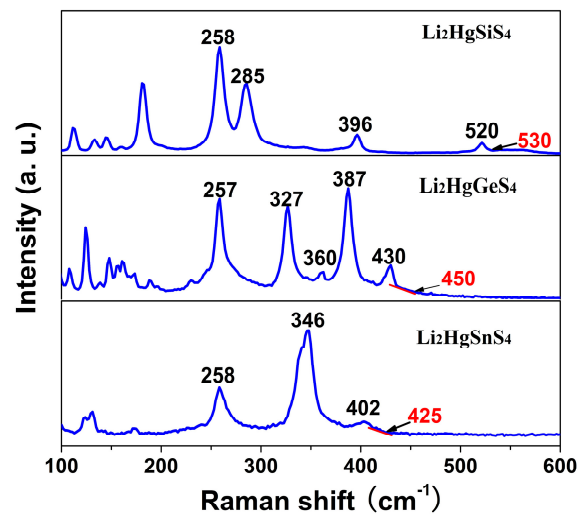
Figure 3. Raman spectra of the title compounds.

Second harmonic generation (SHG) responses for the title compounds were investigated on powder samples and the results are shown in Figure 4. From this figure, it can be found that the SHG intensities of the title compounds are not enhanced gradually with the increase of particle sizes, which indicates the nonphase matching behaviour for these compounds. In addition, their SHG responses are about 0.8 for Li$_2$HgSiS$_4$, 3.0 for Li$_2$HgGeS$_4$, and 4.0 for Li$_2$HgSnS$_4$ times that of benchmark AgGaS$_2$ at the 55–88 μm particle size, respectively, which shows that the title compounds may have great NLO potential in the IR region as promising frequency-conversion candidates.
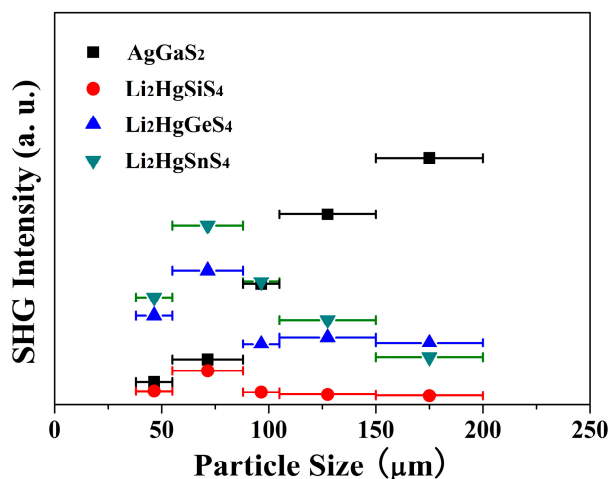
Figure 4. Second-harmonic generation (SHG) intensity versus particle size for the title compounds and $AgGaS_2$.

3. Materials and Methods

3.1. Synthesis

All the starting materials were used as purchased without further refinement. In the preparation process, a graphite crucible was added into the vacuum sealed silica tube to avoid the reaction between metal Li and the silica tube at a high temperature.

3.1.1. Li_2HgSiS_4 and Li_2HgSnS_4

Target compounds were prepared with a mixture with the ratio of Li:HgS:(Si or Sn):S = 2:1:1:3, respectively. The temperature process was set as follows: first, it was heated to 700 °C in two days, and kept at this temperature about four days, then slowly down to 300 °C within four days, and finally quickly cooled to room temperature by turning off the furnace. Obtained products were washed by the *N,N*-dimethylformamide (DMF) solvent to remove the other byproducts. Yellow crystals for Li_2HgSiS_4 and orange-red crystals for Li_2HgSnS_4 appeared, and both of them remained stable in air over half a year. In addition, the yield of Li_2HgSiS_4 was about 80%.

3.1.2. Li_2HgGeS_4

Initially, we attempted to prepare Li_2HgGeS_4 with the ratio of Li:HgS:Ge:S = 2:1:1:3 at the reaction temperature of 700 °C. After the single crystal X-ray diffraction measurement, $Li_4HgGe_2S_7$ (main product, yellow) [79] and Li_2HgGeS_4 (a small amount, reddish) were interestingly obtained. In addition, we had further adjusted the ratio of reactants and interestingly found that the pure-phase of Li_2HgGeS_4 could be obtained while the ratio of Li:HgS is greater than 2:1. Moreover, the Li_2HgGeS_4 crystals were repeatedly washed with DMF solvent and they also remained stable in air.

3.2. Structure Determination

Selected single-crystals were used for data collections with a Bruker SMART APEX II 4K CCD diffractometer (Bruker Corporation, Madison, WI, USA) using Mo Kα radiation (λ = 0.71073 Å) at room temperature. Multi-scan method was used for absorption correction [91]. All the crystal structures were solved by the direct method and refined using the SHELXTL program package [92]. As for the structural refinement of Li_2HgSiS_4, the initial refinement result gave the formula Li_2HgSiS_4, but the site of the Li atom showed abnormal anisotropy parameter (almost zero). Thus, we attempted to set the Li1 and Hg2 atoms to occupy the same site with the ratio of 0.97:0.03 (Li1:Hg2) by random refinement. In view of the low occupancy (0.025) of Hg2 atom, we consider using the "ISOR" order to treat the Li1 atom as isotropic instead of a positional disorder (Li1:Hg2). Moreover, the subsequent

analysis of the element contents in the title compounds with energy dispersive X-ray (EDX) equipped Hitachi S-4800 SEM (Tokyo, Japan) showed the approximate molar ratio of 1:1:4 for Hg, Si/Ge/Sn, and S (Li is undetectable in EDX). The final structures were carefully checked with PLATON software (Glasgow, UK) and no other symmetries were found [93]. Table 3 shows the crystal data and structure refinement of the title compounds.

Table 3. Crystal data and structure refinement for the title compounds.

Empirical Formula	Li_2HgSiS_4	Li_2HgGeS_4	Li_2HgSnS_4
fw	370.80	415.30	461.40
crystal system	*orthorhombic*	*orthorhombic*	*orthorhombic*
space group	$Pmn2_1$	$Pmn2_1$	$Pmn2_1$
a (Å)	7.592 (2)	7.709 (9)	7.9400 (17)
b (Å)	6.7625 (19)	6.812 (8)	6.9310 (15)
c (Å)	6.3295 (18)	6.384 (7)	6.5122 (14)
Z, V (Å^3)	2, 324.96 (16)	2, 335.3 (7)	2, 358.38 (13)
D_c (g/cm^3)	3.790	4.114	4.276
μ (mm^{-1})	25.014	28.463	25.918
GOF on F^2	1.022	1.161	0.985
R_1, wR_2 (I > 2σ(I)) [a]	0.0217, 0.0443	0.0422, 0.0994	0.0318, 0.0633
R_1, wR_2 (all data)	0.0229, 0.0445	0.0438, 0.0999	0.0423, 0.0682
absolute structure parameter	0.003 (11)	0.04 (3)	−0.019 (19)
largest diff. peak and hole (e Å^{-3})	1.318, −1.170	5.723, −1.070	0.959, −1.797

[a] $R_1 = F_o − F_c/F_o$ and $wR_2 = [w (F_o^2 − F_c^2)^2/wF_o^4]^{1/2}$ for $F_o^2 > 2\sigma (F_o^2)$.

3.3. Powder XRD Measurement

A Bruker D2 X-ray diffractometer (Madison, USA) with Cu Kα radiation (λ = 1.5418 Å) was used to measure the powder X-ray diffraction (XRD) patterns of title compounds at room temperature. The measured range is 10–70° with a step size of 0.02°. Compared with the calculated and experiment results, it can be concluded that they are basically consistent with each other, except for Li_2HgSiS_4 with a small number of the Hg_4SiS_4 impurities (Figure 5).
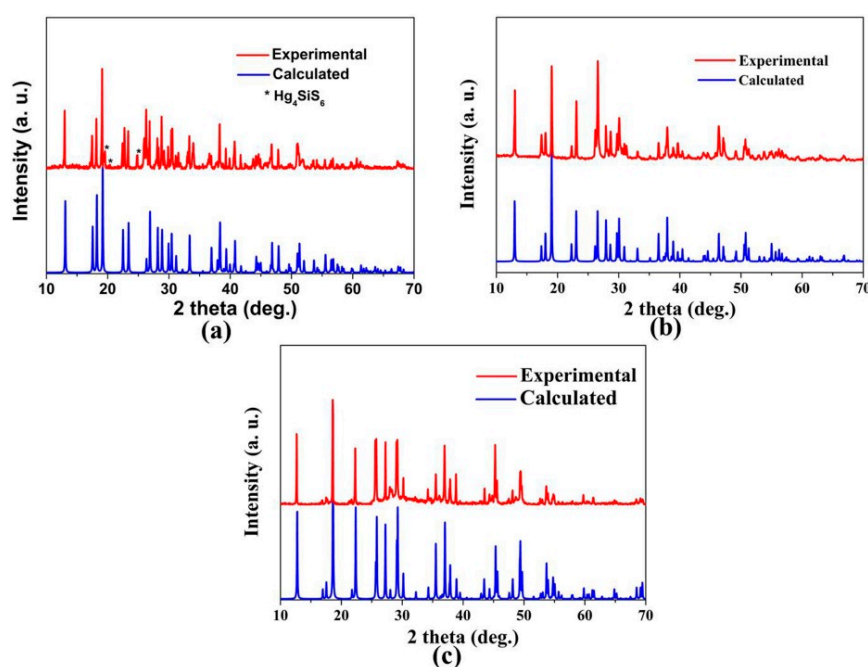
Figure 5. Powder XRD patterns of Li_2HgSiS_4 (**a**), Li_2HgGeS_4 (**b**), Li_2HgSnS_4 (**c**).

3.4. UV–Vis–NIR Diffuse-Reflectance Spectroscopy

Diffuse-reflectance spectra were measured by a Shimadzu SolidSpec-3700DUV spectrophotometer (Shimadzu Corporation, Beijing, China) in the wavelength range of 190–2600 nm at room temperature. The absorption spectra were converted from the reflection spectra via the Kubelka–Munk function.

3.5. Raman Spectroscopy

Hand-picked crystals were first put on an object slide, and then a LABRAM HR Evolution spectrometer equipped with a CCD detector (HORIBA Scientific, Beijing, China) by a 532-nm laser was used to record the Raman spectra. The integration time was set to be 10 s.

3.6. Second-Harmonic Generation Measurement

By the Kurtz and Perry method, powder SHG responses of the title compounds were investigated by a Q-switch laser (2.09 μm, 3 Hz, 50 ns) with ground micro-crystals on different particle sizes. $AgGaS_2$ single-crystal was also ground and sieved into the same size range as the reference. SHG signals were detected by a digital oscilloscope.

3.7. LDT Measurement

Ground micro-crystals samples (55–88 μm) were used to evaluate the LDTs of the title compounds under a pulsed YAG laser (1.06 μm, 10 ns, 10 Hz). Similar sizes of the $AgGaS_2$ crystal were chosen as the reference. By adjusting the laser output energy, colour change of the test sample was carefully observed by an optical microscope to determine the LDTs.

4. Conclusions

A new family of new DLSs, Li_2HgMS_4 (M = Si, Ge, Sn), were successfully synthesized by the solid-state method in vacuum-sealed silica tubes. They are isostructural and crystallize in the orthorhombic *Pmn*2_1 space group. Seen from their structures, they have the similar 3D framework and 2D honeycomb-like layer structures with the interconnection of three types of tetrahedral units (LiS_4, HgS_4, and MS_4). Corresponding optical properties for the title compounds are systemically studied and the results show that they have great potential as promising IR NLO candidates.

Supplementary Materials: The following are available online at www.mdpi.com/2073-4352/7/4/107/s1. Cifs for title compounds.

Author Contributions: Kui Wu conceived and designed this study, prepared the crystals and wrote the manuscript. Shilie Pan conceived and coordinated the project.

Conflicts of Interest: The authors declare no conflict of interest.

References

1.　Keller, U. Recent developments in compact ultrafast lasers. *Nature* **2003**, *424*, 831–838. [CrossRef] [PubMed]
2.　Byer, R.L. Diode laser-pumped solid-state lasers. *Science* **1988**, *239*, 742–748. [CrossRef] [PubMed]
3.　Duarte, F.J. *Tunable Laser Applications*, 2nd ed.; CRC Press: Boca Raton, FL, USA, 2008; Chapters 2, 9 and 12.
4.　Demtröder, W. *Laser Spectroscopy*, 3rd ed.; Springer: Berlin, Germany, 2009.
5.　Nikogosyan, D.N. *Nonlinear Optical Crystals: A Complete Survey*, 1st ed.; Springer: New York, NY, USA, 2005.
6.　Chen, C.T.; Wu, Y.C.; Jiang, A.D.; Wu, B.C.; You, G.M.; Li, R.K.; Lin, S.J. New Nonlinear-Optical Crystal: LiB_3O_5. *J. Opt. Soc. Am. B* **1989**, *6*, 616–621. [CrossRef]
7.　Chen, C.T.; Wu, B.C.; Jiang, A.D.; You, G.M. A New-Type Ultraviolet SHG Crystal-β-BaB_2O_4. *Sci. Sin. Ser. B* **1985**, *28*, 235–243.

8. Mei, L.; Wang, Y.; Chen, C.T.; Wu, B.C. Nonlinear Optical Materials Based on $MBe_2BO_3F_2$ (M = Na, K). *J. Appl. Phys.* **1993**, *74*, 7014–7016. [CrossRef]

9. Wang, G.L.; Zhang, C.Q.; Chen, C.T.; Yao, A.Y.; Zhang, J.; Xu, Z.Y.; Wang, J.Y. High-Efficiency 266-nm Output of a $KBe_2BO_3F_2$ Crystal. *Appl. Opt.* **2003**, *42*, 4331–4334. [CrossRef] [PubMed]

10. Becker, P. Borate Materials in Nonlinear Optics. *Adv. Mater.* **1998**, *10*, 979–992. [CrossRef]

11. Sun, C.F.; Hu, C.L.; Xu, X.; Ling, J.B.; Hu, T.; Kong, F.; Long, X.F.; Mao, J.G. $BaNbO(IO_3)_5$: A New Polar Material with A Very Large SHG Response. *J. Am. Chem. Soc.* **2009**, *131*, 9486–9487. [CrossRef] [PubMed]

12. Hu, C.L.; Mao, J.G. Recent Advances on Second-Order NLO Materials Based on Metal Iodates. *Coord. Chem. Rev.* **2015**, *288*, 1–17. [CrossRef]

13. Song, J.L.; Hu, C.L.; Xu, X.; Kong, F.; Mao, J.G. A Facile Synthetic Route to a New SHG Material with Two Types of Parallel π-Conjugated Planar Triangular Units. *Angew. Chem. Int. Ed.* **2015**, *54*, 3679–3682. [CrossRef] [PubMed]

14. Zou, G.H.; Ye, N.; Huang, L.; Lin, X.S. Alkaline-Alkaline Earth Fluoride Carbonate Crystals $ABCO_3F$ (A = K, Rb, Cs; B = Ca, Sr, Ba) as Nonlinear Optical Materials. *J. Am. Chem. Soc.* **2011**, *133*, 20001–20007. [CrossRef] [PubMed]

15. Yang, G.S.; Peng, G.; Ye, N.; Wang, J.Y.; Luo, M.; Yan, T.; Zhou, Y.Q. Structural Modulation of Anionic Group Architectures by Cations to Optimize SHG Effects: A Facile Route to New NLO Materials in the $ATCO_3F$ (A = K, Rb; T = Zn, Cd) Series. *Chem. Mater.* **2015**, *27*, 7520–7530. [CrossRef]

16. Zou, G.H.; Huang, L.; Ye, N.; Lin, C.S.; Cheng, W.D.; Huang, H. $CsPbCO_3F$: A Strong Second-Harmonic Generation Material Derived from Enhancement via p–π Interaction. *J. Am. Chem. Soc.* **2013**, *135*, 18560–18566. [CrossRef] [PubMed]

17. Yu, H.W.; Zhang, W.G.; Young, J.; Rondinelli, J.M.; Halasyamani, P.S. Bidenticity-Enhanced Second Harmonic Generation from Pb Chelation in $Pb_3Mg_3TeP_2O_{14}$. *J. Am. Chem. Soc.* **2016**, *138*, 88–91. [CrossRef] [PubMed]

18. Yu, H.W.; Zhang, W.G.; Young, J.; Rondinelli, J.M.; Halasyamani, P.S. Design and Synthesis of the Beryllium-Free Deep-Ultraviolet Nonlinear Optical Material $Ba_3(ZnB_5O_{10})PO_4$. *Adv. Mater.* **2015**, *27*, 7380–7385. [CrossRef] [PubMed]

19. Kim, H.G.; Tran, T.T.; Choi, W.; You, T.S.; Halasyamani, P.S.; Ok, K.M. Two New Non-centrosymmetric *n* = 3 Layered Dion–Jacobson Perovskites: Polar $RbBi_2Ti_2NbO_{10}$ and Nonpolar $CsBi_2Ti_2TaO_{10}$. *Chem. Mater.* **2016**, *28*, 2424–2432. [CrossRef]

20. Zou, G.H.; Nam, G.; Kim, H.G.; Jo, H.; You, T.S.; Ok, K.M. $ACdCO_3F$ (A = K and Rb): New Noncentrosymmetric Materials with Remarkably Strong Second-Harmonic Generation (SHG) Responses Enhanced via π-Interaction. *RSC Adv.* **2015**, *5*, 84754–84761. [CrossRef]

21. Cheng, L.; Wei, Q.; Wu, H.Q.; Zhou, L.J.; Yang, G.Y. $Ba_3M_2[B_3O_6(OH)]_2[B_4O_7(OH)_2]$ (M = Al, Ga): Two Novel UV Nonlinear Optical Metal Borates Containing Two Types of Oxoboron Clusters. *Chem. Eur. J.* **2013**, *19*, 17662–17667. [CrossRef] [PubMed]

22. Huang, H.W.; Liu, L.J.; Jin, S.F.; Yao, W.J.; Zhang, Y.H.; Chen, C.T. Deep-Ultraviolet Nonlinear Optical Materials: $Na_2Be_4B_4O_{11}$ and $LiNa_5Be_{12}B_{12}O_{33}$. *J. Am. Chem. Soc.* **2013**, *135*, 18319–18322. [CrossRef] [PubMed]

23. Li, F.; Hou, X.L.; Pan, S.L.; Wang, X.A. Growth, structure, and optical properties of a congruent melting oxyborate, $Bi_2ZnOB_2O_6$. *Chem. Mater.* **2009**, *21*, 2846–2850. [CrossRef]

24. Wu, H.P.; Pan, S.L.; Poeppelmeier, K.R.; Li, H.Y.; Jia, D.Z.; Chen, Z.H.; Fan, X.Y.; Yang, Y.; Rondinelli, J.M.; Luo, H. $K_3B_6O_{10}Cl$: A New Structure Analogous to Perovskite with A Large Second Harmonic Generation Response and Deep UV Absorption Edge. *J. Am. Chem. Soc.* **2011**, *133*, 7786–7790. [CrossRef] [PubMed]

25. Yu, H.W.; Wu, H.P.; Pan, S.L.; Yang, Z.H.; Hou, X.L.; Su, X.; Jing, Q.; Poeppelmeier, K.R.; Rondinelli, J.M. $Cs_3Zn_6B_9O_{21}$: A Chemically Benign Member of the KBBF Family Exhibiting the Largest Second Harmonic Generation Response. *J. Am. Chem. Soc.* **2014**, *136*, 1264–1267. [CrossRef] [PubMed]

26. Li, L.; Wang, Y.; Lei, B.H.; Han, S.J.; Yang, Z.H.; Poeppelmeier, K.R.; Pan, S.L. A New Deep-Ultraviolet Transparent Orthophosphate $LiCs_2PO_4$ with Large Second Harmonic Generation Response. *J. Am. Chem. Soc.* **2016**, *138*, 9101–9104. [CrossRef] [PubMed]

27. Wang, Y.; Pan, S.L. Recent Development of Metal Borate Halides: Crystal Chemistry and Application in Second-order NLO Materials. *Coord. Chem. Rev.* **2016**, *323*, 15–35. [CrossRef]

28. Dong, X.Y.; Jing, Q.; Shi, Y.J.; Yang, Z.H.; Pan, S.L.; Poeppelmeier, K.R.; Young, J.S.; Rondinelli, J.M. $Pb_2Ba_3(BO_3)_3Cl$: A Material with Large SHG Enhancement Activated by Pb-Chelated BO_3 Groups. *J. Am. Chem. Soc.* **2015**, *137*, 9417–9422. [CrossRef] [PubMed]

29. Wu, H.P.; Yu, H.W.; Pan, S.L.; Huang, Z.J.; Yang, Z.H.; Su, X.; Poeppelmeier, K.R. $Cs_2B_4SiO_9$, A Deep-ultraviolet Nonlinear Optical Crystal. *Angew. Chem. Int. Ed.* **2013**, *52*, 3406–3410. [CrossRef] [PubMed]

30. Wu, H.P.; Yu, H.W.; Yang, Z.H.; Hou, X.L.; Su, X.; Pan, S.L.; Poeppelmeier, K.R.; Rondinelli, J.M. Designing a Deep-Ultraviolet Nonlinear Optical Material with a Large Second Harmonic Generation Response. *J. Am. Chem. Soc.* **2013**, *135*, 4215–4218. [CrossRef] [PubMed]

31. Zhao, S.; Gong, P.; Bai, L.; Xu, X.; Zhang, S.; Sun, Z.; Lin, Z.; Hong, M.; Chen, C.; Luo, J. Beryllium-free $Li_4Sr(BO_3)_2$ for Deep-ultraviolet Nonlinear Optical Applications. *Nat. Commun.* **2014**, *5*. [CrossRef] [PubMed]

32. Zhao, S.G.; Gong, P.F.; Luo, S.Y.; Bai, L.; Lin, Z.S.; Tang, Y.Y.; Zhou, Y.L.; Hong, M.C.; Luo, J.H. Tailored Synthesis of a Nonlinear Optical Phosphate with a Short Absorption Edge. *Angew. Chem. Int. Ed.* **2015**, *54*, 4217–4221. [CrossRef] [PubMed]

33. Zhao, S.G.; Gong, P.F.; Luo, S.Y.; Liu, S.J.; Li, L.N.; Asghar, M.A.; Khan, T.; Hong, M.C.; Lin, Z.S.; Luo, J.H. Beryllium-Free $Rb_3Al_3B_3O_{10}F$ with Reinforced Inter layer Bonding as a Deep-Ultraviolet Nonlinear Optical Crystal. *J. Am. Chem. Soc.* **2015**, *137*, 2207–2210. [CrossRef] [PubMed]

34. Jiang, X.X.; Luo, S.Y.; Kang, L.; Gong, P.F.; Huang, H.W.; Wang, S.C.; Lin, Z.S.; Chen, C.T. First-Principles Evaluation of the Alkali and/or Alkaline Earth Beryllium Borates in Deep Ultraviolet Nonlinear Optical Applications. *ACS Photonics* **2015**, *2*, 1183–1191. [CrossRef]

35. Okorogu, A.O.; Mirov, S.B.; Lee, W.; Crouthamel, D.I.; Jenkins, N.; Dergachev, A.Y.; Vodopyanov, K.L.; Badikov, V.V. Tunable Middle Infrared Downconversion in GaSe and $AgGaS_2$. *Opt. Commun.* **1998**, *155*, 307–312. [CrossRef]

36. Boyd, G.D.; Storz, F.G.; McFee, J.H.; Kasper, H.M. Linear and Nonlinear Optical Properties of Some Ternary Selenides. *IEEE J. Quantum Electron.* **1972**, *8*, 900–908. [CrossRef]

37. Boyd, G.D.; Buehler, E.; Storz, F.G. Linear and Nonlinear Optical Properties of $ZnGeP_2$ and CdSe. *Appl. Phys. Lett.* **1971**, *18*, 301–304. [CrossRef]

38. Chung, I.; Kanatzidis, M.G. Metal chalcogenides: A rich source of nonlinear optical materials. *Chem. Mater.* **2014**, *26*, 849–869. [CrossRef]

39. Jiang, X.M.; Guo, S.P.; Zeng, H.Y.; Zhang, M.J.; Guo, G.C. Large Crystal Growth and New Crystal Exploration of Mid-Infrared Second-Order Nonlinear Optical Materials. *Struct. Bond.* **2012**, *145*, 1–43.

40. Liang, F.; Kang, L.; Lin, Z.S.; Wu, Y.C.; Chen, C.T. Analysis and Prediction of Mid-IR Nonlinear Optical Metal Sulfides with Diamond-like Structures. *Coord. Chem. Rev.* **2017**, *333*, 57–70. [CrossRef]

41. Guo, S.P.; Chi, Y.; Guo, G.C. Recent Achievements on Middle and Far-infrared Second-order Nonlinear Optical Materials. *Coord. Chem. Rev.* **2017**, *335*, 44–57. [CrossRef]

42. Bera, T.K.; Jang, J.I.; Ketterson, J.B.; Kanatzidis, M.G. Strong Second Harmonic Generation from the Tantalum Thioarsenates $A_3Ta_2AsS_{11}$ (A = K and Rb). *J. Am. Chem. Soc.* **2009**, *131*, 75–77. [CrossRef] [PubMed]

43. Zhang, W.; Li, F.; Kim, S.H.; Halasyamani, P.S. Top-Seeded Solution Crystal Growth and Functional Properties of a Polar Material $Na_2TeW_2O_9$. *Cryst. Growth Des.* **2010**, *10*, 4091–4095. [CrossRef]

44. Lin, H.; Zhou, L.J.; Chen, L. Sulfides with Strong Nonlinear Optical Activity and Thermochromism: $ACd_4Ga_5S_{12}$ (A = K, Rb, Cs). *Chem. Mater.* **2012**, *24*, 3406–3414. [CrossRef]

45. Chen, M.C.; Wu, L.M.; Lin, H.; Zhou, L.J.; Chen, L. Disconnection Enhances the Second Harmonic Generation Response: Synthesis and Characterization of $Ba_{23}Ga_8Sb_2S_{38}$. *J. Am. Chem. Soc.* **2012**, *134*, 6058–6060. [CrossRef] [PubMed]

46. Yu, P.; Zhou, L.J.; Chen, L. Noncentrosymmetric Inorganic Open-Framework Chalcohalides with Strong Middle IR SHG and Red emission: $Ba_3AGa_5Se_{10}Cl_2$ (A = Cs, Rb, K). *J. Am. Chem. Soc.* **2012**, *134*, 2227–2235. [CrossRef] [PubMed]

47. Chen, M.C.; Li, L.H.; Chen, Y.B.; Chen, L. In-Phase Alignments of Asymmetric Building Units in Ln_4GaSbS_9 (Ln = Pr, Nd, Sm, Gd–Ho) and Their Strong Nonlinear Optical Responses in Middle IR. *J. Am. Chem. Soc.* **2011**, *133*, 4617–4624. [CrossRef] [PubMed]

48. Chen, Y.K.; Chen, M.C.; Zhou, L.J.; Chen, L.; Wu, L.M. Syntheses, Structures, and Nonlinear Optical Properties of Quaternary Chalcogenides: $Pb_4Ga_4GeQ_{12}$ (Q = S, Se). *Inorg. Chem.* **2013**, *52*, 8334–8341. [CrossRef] [PubMed]

49. Yao, J.Y.; Mei, D.J.; Bai, L.; Lin, Z.S.; Yin, W.L.; Fu, P.Z.; Wu, Y.C. $BaGa_4Se_7$: A New Congruent-Melting IR Nonlinear Optical Material. *Inorg. Chem.* **2010**, *49*, 9212–9216. [CrossRef] [PubMed]

50. Lin, X.S.; Zhang, G.; Ye, N. Growth and Characterization of $BaGa_4S_7$: A New Crystal for Mid-IR Nonlinear Optics. *Cryst. Growth Des.* **2009**, *9*, 1186–1189. [CrossRef]

51. Luo, Z.Z.; Lin, C.S.; Cui, H.H.; Zhang, W.L.; Zhang, H.; Chen, H.; He, Z.Z.; Cheng, W.D. $PbGa_2MSe_6$ (M = Si, Ge): Two Exceptional Infrared Nonlinear Optical Crystals. *Chem. Mater.* **2015**, *27*, 914–922. [CrossRef]

52. Luo, Z.Z.; Lin, C.S.; Cui, H.H.; Zhang, W.L.; Zhang, H.; He, Z.Z.; Cheng, W.D. SHG Materials $SnGa_4Q_7$ (Q = S, Se) Appearing with Large Conversion Efficiencies, High Damage Thresholds, and Wide Transparencies in the Mid-Infrared Region. *Chem. Mater.* **2014**, *26*, 2743–2749. [CrossRef]

53. Geng, L.; Cheng, W.D.; Lin, C.S.; Zhang, W.L.; Zhang, H.; He, Z.Z. Syntheses and Characterization of New Mid-Infrared Transparency Compounds: Centric Ba_2BiGaS_5 and Acentric Ba_2BiInS_5. *Inorg. Chem.* **2011**, *50*, 5679–5686. [CrossRef] [PubMed]

54. Luo, Z.Z.; Lin, C.S.; Zhang, W.L.; Zhang, H.; He, Z.Z.; Cheng, W.D. $Ba_8Sn_4S_{15}$: A Strong Second Harmonic Generation Sulfide with Zero-Dimensional Crystal Structure. *Chem. Mater.* **2013**, *26*, 1093–1099. [CrossRef]

55. Liu, B.W.; Zeng, H.Y.; Zhang, M.J.; Fan, Y.H.; Guo, G.C.; Huang, J.S.; Dong, Z.C. Syntheses, Structures, and Nonlinear-optical Properties of Metal Sulfides $Ba_2Ga_8MS_{16}$ (M = Si, Ge). *Inorg. Chem.* **2014**, *54*, 976–981. [CrossRef] [PubMed]

56. Li, S.F.; Liu, B.W.; Zhang, M.J.; Fan, Y.H.; Zeng, H.Y.; Guo, G.C. Syntheses, Structures, and Nonlinear Optical Properties of Two Sulfides $Na_2In_2MS_6$ (M = Si, Ge). *Inorg. Chem.* **2016**, *55*, 1480–1485. [CrossRef] [PubMed]

57. Wu, Q.; Meng, X.G.; Zhong, C.; Chen, X.G.; Qin, J.G. $Rb_2CdBr_2I_2$: A New IR Nonlinear Optical Material with a Large Laser Damage Threshold. *J. Am. Chem. Soc.* **2014**, *136*, 5683–5686. [CrossRef] [PubMed]

58. Zhang, G.; Li, Y.J.; Jiang, K.; Zeng, H.Y.; Liu, T.; Chen, X.G.; Qin, J.G.; Lin, Z.S.; Fu, P.Z.; Wu, Y.C.; et al. A New Mixed Halide, $Cs_2HgI_2Cl_2$: Molecular Engineering for a New Nonlinear Optical Material in the Infrared Region. *J. Am. Chem. Soc.* **2012**, *134*, 14818–14822. [CrossRef] [PubMed]

59. Haynes, A.S.; Saouma, F.O.; Otieno, C.O.; Clark, D.J.; Shoemaker, D.P.; Jang, J.I.; Kanatzidis, M.G. Phase-Change Behavior and Nonlinear Optical Second and Third Harmonic Generation of The One-Dimensional $K_{(1-x)}Cs_xPSe_6$ and Metastable β-$CsPSe_6$. *Chem. Mater.* **2015**, *27*, 1837–1846. [CrossRef]

60. Wu, K.; Yang, Z.H.; Pan, S.L. $Na_4MgM_2Se_6$ (M = Si, Ge): The First Noncentrosymmetric Compounds with Special Ethane-Like $[M_2Se_6]^{6-}$ Units Exhibiting Large Laser-Damage Thresholds. *Inorg. Chem.* **2015**, *54*, 10108–10110. [CrossRef] [PubMed]

61. Wu, K.; Yang, Z.H.; Pan, S.L. $Na_2Hg_3M_2S_8$ (M = Si, Ge, and Sn): New Infrared Nonlinear Optical Materials with Strong Second Harmonic Generation Effects and High Laser-Damage Thresholds. *Chem. Mater.* **2016**, *28*, 2795–2801. [CrossRef]

62. Wu, K.; Yang, Z.H.; Pan, S.L. Na_2BaMQ_4 (M =Ge, Sn; Q=S, Se): Infrared Nonlinear Optical Materials with Excellent Performances and that Undergo Structural Transformations. *Angew. Chem. Int. Ed.* **2016**, *128*, 6825–6827. [CrossRef]

63. Zhen, N.; Nian, L.Y.; Li, G.M.; Wu, K.; Pan, S.L. A High Laser Damage Threshold and a Good Second-Harmonic Generation Response in a New Infrared NLO Material: $LiSm_3SiS_7$. *Crystals* **2016**, *6*, 121. [CrossRef]

64. Li, G.M.; Wu, K.; Liu, Q.; Yang, Z.H.; Pan, S.L. $Na_2ZnGe_2S_6$: A New Infrared Nonlinear Optical Material with Good Balance between Large Second-Harmonic Generation Response and High Laser Damage Threshold. *J. Am. Chem. Soc.* **2016**, *138*, 7422–7428. [CrossRef] [PubMed]

65. Pan, M.Y.; Ma, Z.J.; Liu, X.C.; Xia, S.Q.; Tao, X.T.; Wu, K.C. $Ba_4AgGa_5Pn_8$ (Pn = P, As): New Pnictide-Based Compounds with Nonlinear Optical Potential. *J. Mater. Chem. C* **2015**, *3*, 9695–9700. [CrossRef]

66. Kuo, S.M.; Chang, Y.M.; Chung, I.; Jang, J.I.; Her, B.H.; Yang, S.H.; Ketterson, J.B.; Kanatzidis, M.G.; Hsu, K.F. New Metal Chalcogenides $Ba_4CuGa_5Q_{12}$ (Q = S, Se) Displaying Strong Infrared Nonlinear Optical Response. *Chem. Mater.* **2013**, *25*, 2427–2433. [CrossRef]

67. Bera, T.K.; Jang, J.I.; Song, J.H.; Malliakas, C.D.; Freeman, A.J.; Ketterson, J.B.; Kanatzidis, M.G. Soluble Semiconductors $AAsSe_2$ (A = Li, Na) with a Direct-Band-Gap and Strong Second Harmonic Generation: A Combined Experimental and Theoretical Study. *J. Am. Chem. Soc.* **2010**, *132*, 3484–3495. [CrossRef] [PubMed]

68. Liao, J.H.; Marking, G.M.; Hsu, K.F.; Matsushita, Y.; Ewbank, M.D.; Borwick, R.; Cunningham, P.; Rosker, M.J.; Kanatzidis, M.G. α- and β-$A_2Hg_3M_2S_8$ (A = K, Rb; M= Ge, Sn): Polar Quaternary Chalcogenides with Strong Nonlinear Optical Response. *J. Am. Chem. Soc.* **2003**, *125*, 9484–9493. [CrossRef] [PubMed]

69. Parthé, E. *Crystal Chemistry of Tetrahedral Structures*; Gordon and Breach Science: New York, NY, USA, 1964.

70. Aitken, J.A.; Larson, P.; Mahanti, S.D.; Kanatzidis, M.G. Li_2PbGeS_4 and Li_2EuGeS_4: Polar Chalcopyrites with a Severe Tetragonal Compression. *Chem. Mater.* **2001**, *13*, 4714–4721. [CrossRef]

71. Bai, L.; Lin, Z.S.; Wang, Z.Z.; Chen, C.T. Mechanism of Linear and Nonlinear Optical Effects of Chalcopyrites $LiGaX_2$ (X = S, Se and Te) Crystals. *J. Appl. Phys.* **2008**, *103*, 083111. [CrossRef]

72. Kim, Y.; Seo, I.S.; Martin, S.W.; Baek, J.; Shiv Halasyamani, P.; Arumugam, N.; Steinfink, H. Characterization of New Infrared Nonlinear Optical Material with High Laser Damage Threshold, $Li_2Ga_2GeS_6$. *Chem. Mater.* **2008**, *20*, 6048–6052. [CrossRef]

73. Shi, Y.F.; Chen, Y.K.; Chen, M.C.; Wu, L.M.; Lin, H.; Zhou, L.J.; Chen, L. Strongest Second Harmonic Generation in the Polar R_3MTQ_7 Family: Atomic Distribution Induced Nonlinear Optical Cooperation. *Chem. Mater.* **2015**, *27*, 1876–1884. [CrossRef]

74. Brant, J.A.; Clark, D.J.; Kim, Y.S.; Jang, J.I.; Zhang, J.H.; Aitken, J.A. Li_2CdGeS_4, A Diamond-Like Semiconductor with Strong Second-Order Optical Nonlinearity in the Infrared and Exceptional Laser Damage Threshold. *Chem. Mater.* **2014**, *26*, 3045–3048. [CrossRef]

75. Brant, J.A.; Clark, D.J.; Kim, Y.S.; Jang, J.I.; Weiland, A.; Aitken, J.A. Outstanding Laser Damage Threshold in Li_2MnGeS_4 and Tunable Optical Nonlinearity in Diamond-Like Semiconductors. *Inorg. Chem.* **2015**, *4*, 2809–2819. [CrossRef] [PubMed]

76. Rosmus, K.A.; Brant, J.A.; Wisneski, S.D.; Clark, D.J.; Kim, Y.S.; Jang, J.I.; Brunetta, C.D.; Zhang, J.H.; Srnec, M.N.; Aitken, J.A. Optical Nonlinearity in Cu_2CdSnS_4 and α/β-Cu_2ZnSiS_4: Diamond-like Semiconductors with High Laser-Damage Thresholds. *Inorg. Chem.* **2014**, *53*, 7809–7811. [CrossRef] [PubMed]

77. Brant, J.A.; Cruz, C.D.; Yao, J.L.; Douvalis, A.P.; Bakas, T.; Sorescu, M.; Aitken, J.A. Field-Induced Spin-Flop in Antiferromagnetic Semiconductors with Commensurate and Incommensurate Magnetic Structures: Li_2FeGeS_4 (LIGS) and Li_2FeSnS_4 (LITS). *Inorg. Chem.* **2014**, *53*, 12265–12274. [CrossRef] [PubMed]

78. Zhang, J.H.; Clark, D.J.; Brant, J.A.; Sinagra, C.W.; Kim, Y.S.; Jang, J.I.; Aitken, J.A. Infrared Nonlinear Optical Properties of Lithium-Containing Diamond-Like Semiconductors $Li_2ZnGeSe_4$ and $Li_2ZnSnSe_4$. *Dalton Trans.* **2015**, *44*, 11212–11222. [CrossRef] [PubMed]

79. Devlin, K.P.; Glaid, A.J.; Brant, J.A.; Zhang, J.H.; Srnec, M.N.; Clark, D.J.; Kim, Y.S.; Jang, J.I.; Daley, K.R.; Moreau, M.A.; et al. Polymorphism and Second Harmonic Generation in a Novel Diamond-Like Semiconductor: Li_2MnSnS_4. *J. Solid State Chem.* **2015**, *231*, 256–266. [CrossRef]

80. Lekse, J.W.; Leverett, B.M.; Lake, C.H.; Aitken, J.A. Synthesis, physicochemical characterization and crystallographic twinning of Li_2ZnSnS_4. *J. Solid State Chem.* **2008**, *181*, 3217–3222. [CrossRef]

81. Rotermund, F.; Petrov, V.; Noack, F. Difference-Frequency Generation of Intense Femtosecond Pulses in the Mid-IR (4–12 μm) Using $HgGa_2S_4$ and $AgGaS_2$. *Opt. Commun.* **2000**, *185*, 177–183. [CrossRef]

82. Wu, K.; Su, X.; Pan, S.L.; Yang, Z.H. Synthesis and Characterization of Mid-Infrared Transparency Compounds: Acentric $BaHgS_2$ and Centric $Ba_8Hg_4S_5Se_7$. *Inorg. Chem.* **2015**, *54*, 2772–2779. [CrossRef] [PubMed]

83. Li, C.; Yin, W.L.; Gong, P.F.; Li, X.X.; Zhou, M.L.; Mar, A.; Lin, Z.S.; Yao, J.Y.; Wu, Y.C.; Chen, C.T. Trigonal Planar $[HgSe_3]^{4-}$ Unit: A New Kind of Basic Functional Group in IR Nonlinear Optical Materials with Large Susceptibility and Physicochemical Stability. *J. Am. Chem. Soc.* **2016**, *138*, 6135–6138. [CrossRef] [PubMed]

84. Wu, K.; Yang, Z.H.; Pan, S.L. The First Quaternary Diamond-like Semiconductor with 10-membered LiS_4 Rings Exhibiting Excellent Nonlinear Optical Performances. *Chem. Commun.* **2017**, *53*, 3010–3013. [CrossRef] [PubMed]

85. I Brese, N.E.; O'Keeffe, M. Bond-Valence Parameters for Solid. *Acta Crystallogr. B* **1991**, *47*, 192–197. [CrossRef]

86. Brown, I.D.; Altermatt, D. Bond-Valence Parameters Obtained from a Systematic Analysis of the Inorganic Crystal Structure Database. *Acta Crystallogr. B* **1985**, *41*, 244–247. [CrossRef]

87. Brown, I.D. *The Chemical Bond in Inorganic Chemistry: The Bond Valence Model*, 1st ed.; Oxford University Press: Oxford, UK, 2002.
88. Preiser, C.; Losel, J.; Brown, I.D.; Kunz, M.; Skowron, A. Long Range Coulomb Forces and Localized Bonds. *Acta Crystallogr. B* **1999**, *55*, 69–711. [CrossRef]
89. Salinas-Sanchez, A.; Garcia-Munoz, J.L.; Rodriguez-Carvajal, J.; Saez-Puche, R.; Martinez, J.L. Structural Characterization of R_2BaCuO_5 (R = Y, Lu, Yb, Tm, Er, Ho, Dy, Gd, Eu and Sm) Oxides by X-ray and Neutron Diffraction. *J. Solid State Chem.* **1992**, *100*, 201–211. [CrossRef]
90. Chen, S.; Walsh, A.; Luo, Y.; Yang, J.H.; Gong, X.G.; Wei, S.H. Wurtzite-Derived Polytypes of Kesterite and Stannite Quaternary Chalcogenide Semiconductors. *Phys. Rev. B* **2010**, *82*, 195203. [CrossRef]
91. Bhar, G.C.; Smith, R.C. Optical Properties of II–IV–V_2 and I–III–VI_2 crystals with Particular Reference to Transmission Limits. *Phys. Status Solidi A* **1972**, *13*, 157–168. [CrossRef]
92. Sheldrick, G.M. *SHELXTL*, version 6.14; Bruker Analytical X-ray Instruments, Inc.: Madison, WI, USA, 2008.
93. Spek, A.L. Single-Crystal Structure Validation with the Program PLATON. *J. Appl. Crystallogr.* **2003**, *36*, 7–13. [CrossRef]